AGU PUBLICATIONS

Water Resources Research

RESEARCH ARTICLE

10.1002/2013WR013604

# A field and modeling study of nonlinear storage-discharge dynamics for an Alpine headwater catchment

**Matteo Camporese[1,2], Daniele Penna[3,4,5], Marco Borga[3], and Claudio Paniconi[6]**

[1]Department of Civil, Environmental, and Architectural Engineering, University of Padua, Padua, Italy, [2]Department of Civil Engineering, Monash University, Clayton, Victoria, Australia, [3]Department of Land, Environment, Agriculture, and Forestry, University of Padua, Padua, Italy, [4]Faculty of Science and Technology, Free University of Bozen-Bolzano, Bolzano, Italy, [5]Now at Department of Environmental Systems Science, Swiss Federal Institute of Technology (ETH), Zurich, Switzerland, [6]Institut National de la Recherche Scientifique, Centre Eau Terre Environnement (INRS-ETE), Université du Québec, Quebec City, Canada

**Key Points:**
- A process-based model reproduces observed nonlinear storage-discharge dynamics
- Streamflow responds faster than groundwater in Alpine headwater catchments
- Hysteresis and thresholding are controlled mainly by topography and soil depth

**Correspondence to:**
M. Camporese,
matteo.camporese@unipd.it

**Citation:**
Camporese, M., D. Penna, M. Borga, and C. Paniconi (2014), A field and modeling study of nonlinear storage-discharge dynamics for an Alpine headwater catchment, *Water Resour. Res.*, *50*, 806–822, doi:10.1002/2013WR013604.

Received 29 JAN 2013
Accepted 2 JAN 2014
Accepted article online 6 JAN 2014
Published online 3 FEB 2014

**Abstract** A process-based coupled model of surface-subsurface flow is applied to the simulation of nonlinear hydrological dynamics for an experimental mountain headwater catchment in northeastern Italy. The comparison between measured and simulated responses, both distributed (water table and soil moisture) and integrated (streamflow at the outlet), shows that the model satisfactorily reproduces various nonlinear processes, in particular threshold behavior and hysteresis in the catchment storage-discharge relationship. We typically observe a clockwise loop in this relationship, i.e., streamflow response is faster than groundwater and soil moisture response, due to larger time scales for subsurface processes and to soil moisture persistence and redistribution. The model is based on a standard Richards equation representation of integrated saturated-unsaturated-runoff dynamics and needs no ad hoc parameterization (e.g., for macropores, pipe flow, or retention curve hysteresis) to capture observed hysteretic relationships between storage and discharge. Additional numerical experiments are carried out to investigate how heterogeneity (bedrock permeability and the distinction between riparian and hillslope areas) and aquifer thickness and topography affect this nonlinear dynamics. The results show that catchment topography and soil depth exert the main control on the hysteresis and threshold patterns. This is evident from a spatial analysis of streamflow and water table response times to storm events, where the threshold points correspond to changes in terrain slope. These findings are confirmed by a further set of analyses carried out on an idealized v-shaped catchment.

## 1. Introduction

Threshold behavior and hysteresis in storage-discharge relationships are common manifestations of nonlinear hydrologic response connected to runoff generation processes at the hillslope and catchment scales [*Dooge*, 2005]. Typically, in hydrological systems, thresholds appear as abrupt changes in a response variable (e.g., outlet discharge, storm runoff, and water table depth) when a certain level or a range of values of a driving variable (e.g., soil moisture, subsurface storage, and storm rainfall) is exceeded. In proximity of a threshold, the system might evolve to a "critical" state [*Phillips*, 2003], and different hydrological processes may become dominant above the threshold. Hysteresis is the dependence of a response variable not only on the current value of a driving variable but on its past history as well. Hysteresis leads to a characteristic "looping" behavior when the two variables are plotted against each other.

Nonlinear dynamics has been extensively analyzed in the hydrological literature. Thresholding has been reported under various climatic and physiographic conditions and in the relationship between several state variables, including discharge and soil moisture [*Zehe et al.*, 2010; *Penna et al.*, 2011; *Radatz et al.*, 2013], water table and soil moisture [*Latron and Gallart*, 2008; *Penna et al.*, 2011], subsurface stormflow and rainfall [*Tromp-van Meerveld and McDonnell*, 2006a, 2006b; *Detty and McGuire* 2010a, 2010b; *Penna et al.*, 2013b], and runoff coefficient and precipitation intensity [*Lehmann et al.*, 2007; *Radatz et al.*, 2013]. Hysteresis is also well documented at different scales and for different process dynamics [*O'Kane and Flynn*, 2007, and references therein]. One of the most frequent manifestations of hysteresis in catchment hydrology arises in the relationship between storage and discharge. In this paper, the term "storage" refers to any variable that


© 2014. American Geophysical Union. All Rights Reserved.

quantifies or reflects the volume of water stored in the subsurface, such as aquifer water level, soil moisture content, saturated zone storage, unsaturated zone storage, or total storage. Hysteresis is also observed in surface water hydrology, as for instance in stage-discharge relationships where, for the same stage height, discharge in the rising limb is greater than in the falling limb [*Mishra and Singh*, 1999]. A conceptually simple model of hysteretic behavior is presented in *O'Kane and Flynn* [2007], where exceedance of a threshold switches the output onto a particular solution branch.

Storage-discharge hysteresis connected to subsurface and rainfall-runoff processes has been documented for a wide array of experimental catchments. *McGlynn et al*. [2004] observed strong water table-runoff looping in the riparian floodplain of a 280 ha subcatchment of the Maimai watershed in New Zealand, with groundwater response lagging catchment runoff response. They found that the degree of hysteresis varied as a function of antecedent wetness and event size, and that for an 80 ha subcatchment and a first-order hillslope (0.5 ha) hysteresis was minimal. *Myrabø* [1997] found that the hysteretic behavior between discharge and groundwater levels in a small forested till catchment in Norway was dependent on location and antecedent conditions. Particularly, he noted that during wet conditions (above a certain value of stream discharge) the hysteresis effect vanished almost simultaneously in all groundwater wells due to the rapid transport mechanisms between the different locations and the catchment outlet. For heavy and persistent rainfall events, a unique function between runoff and groundwater was obtained. These results agree with recent findings by *Weill et al*. [2013] who showed, for a small pre-Alpine catchment in Italy, that the storage–streamflow hysteresis relationship was dependent on the mean saturation of the catchment, with higher degrees of saturation tending to yield one-to-one relationships between streamflow and water storage. They obtained looping behavior when plotting the extent of connected saturated area against streamflow, as well as subsurface storage against streamflow. Similarly, *Allen et al*. [2010], analyzing groundwater level and streamflow for nine observation wells in temperate mountainous terrain in British Columbia (Canada), speculated that the pattern of the discharge-water level relationship was a function of the connectivity between the aquifer and the stream. They concluded that the recharge and discharge response of the groundwater system was dependent not only on the storage and permeability characteristics of the aquifer but also on whether the system was stream-driven or recharge-driven. *Kendall et al*. [1999] found hysteresis in the groundwater level-streamflow relationship during snowmelt events for the 41 ha forested headwater catchment at Sleepers River in Vermont. Similarly to *Myrabø* [1997], they identified different patterns according to well location. In riparian zones, the loops were counterclockwise (higher groundwater level for given discharge on the rising limb than for the same discharge on the falling limb) while on the hillslope they were clockwise (groundwater response lagged the streamflow increase). An analogous loop inversion was reported by *Penna et al*. [2011] in the streamflow-soil moisture relationship for an Alpine headwater catchment. These authors observed that during rainfall events with dry antecedent conditions, streamflow responded and peaked earlier than hillslope soil moisture (clockwise loops), while for events with wet antecedent conditions, streamflow lagged soil moisture (counterclockwise loops).

A few authors have attempted to simulate the hysteresis effect between storage and runoff in order to better understand catchment response dynamics. *Ewen and Birkinshaw* [2007] developed a lumped hysteretic subsurface stormflow model for the 0.94 $km^2$ Slapton Wood catchment in the UK and found that the basic pattern of storage-runoff hysteresis was anticlockwise, which the model reproduced reasonably well for large delayed responses but less well for small delays. *Norbiato and Borga* [2008], analyzing storage-flux hysteretic behavior at the hillslope scale with a kinematic wave model, obtained both clockwise and anticlockwise loop cycles and related the increase in hysteresis to the increasing convergence and concavity of the hillslopes. *Frei et al*. [2010] focused on the effects of microtopography on surface-subsurface exchange and runoff generation for a riparian wetland system in a small mountain catchment in southeast Germany. These authors performed virtual modeling experiments and identified distinctly different behaviors of the system during wetting and drying that resulted in marked anticlockwise hysteretic loops between streamflow and riparian groundwater level, matching well the experimental data.

Nonlinear processes in mountain catchments, and particularly headwater catchments, are often related to the complex topographic features that characterize these environments. Different temporal dynamics on the hillslope and in the riparian zone are often found to be responsible for threshold effects or hysteretic behaviors [e.g., *Sidle et al*., 2000; *McGlynn et al*., 2004; *Penna et al*., 2010, 2011]. Hillslopes are thought to be the main contributors to streamflow [*Seibert et al*., 2009; *McGuire and McDonnell*, 2010; *Vidon*, 2011], even


© 2014. American Geophysical Union. All Rights Reserved.

though riparian areas respond faster to precipitation due to higher antecedent soil moisture and shallower water tables near the stream. The hillslope contribution relies on the establishment of a hillslope-riparian hydrological connection that allows rapid displacement of groundwater to the stream [*Wenninger et al*., 2004]. In addition to topographic differences, the riparian corridor and the hillslope tend to have different soil and vegetation properties [*Hill*, 1996]. Understanding the nonlinear interactions between these two zones thus has important ecological as well as hydrological implications.

In this paper, we investigate threshold effects and hysteretic dynamics of storage-discharge relationships for the Larch Creek catchment (LCC), a 3.3 ha headwater catchment in the Italian Alps. Our main goals are (i) to identify the dominant controls on nonlinear processes involved in runoff generation at LCC and (ii) to determine whether a Richards equation (RE)-based hydrological model is able to reproduce the complex behavior (strong nonlinearity, hysteresis, and thresholding) observed at LCC without needing to explicitly represent hysteresis in soil characteristics, macropore flow, fingering, or other possible controlling mechanisms [e.g., *Beven*, 2006] that may require an ad hoc parameterization. The study is undertaken by means of a process-based hydrological model of surface-subsurface flow calibrated and validated against a comprehensive data set of field measurements. The model couples a 3-D RE solver with an inertia-free approximation of the Saint Venant equations for surface flow [*Camporese et al*., 2010] and has been shown to be a suitable tool for simulating hydrological processes over a range of spatial and temporal scales [*Bixio et al*., 2002; *Gauthier et al*., 2009; *Sulis et al*., 2011a, 2011b; *Guay et al*., 2013]. The model is general enough in its treatment of topography, parameter heterogeneity, domain geometry, and boundary conditions to allow close representation of the LCC, including the distinction between riparian and hillslope zones and the possibility of bedrock leakage. In addition to full treatment of the unsaturated zone, the use of a process-based distributed model in this study allows various components of subsurface storage to be readily quantified (soil water content, groundwater levels, and total volume of water in the unsaturated, saturated, and entire subsurface domains). To quantify the influence of the catchment topographic structure (e.g., ratio between the extent of the hillslope and riparian zones) on the nonlinear relationship between storage and discharge, the RE-based model is also applied to an idealized v-shaped catchment in three different configurations. These synthetic simulations allow us to strip away some of the real world complexity of the LCC and isolate the main factors that control the nonlinear storage-discharge relationship.

The paper is organized as follows. After a short description of the study area and of the hydrological model in section 2, section 3 reports on the model simulations of the LCC and discusses the capability of the model to reproduce the observed nonlinear storage-discharge response. In sections 4 and 5, we seek to isolate the main factors controlling this response, via a series of numerical experiments carried out first on the LCC but with different configurations of soil thickness and lateral zonation, and then on the v-catchment.

## 2. Materials and Methods

### 2.1. Field Study and Measurements

Field data were collected in the 3.3 ha LCC (Figure 1), located in the Dolomites (eastern Italian Alps). The area is characterized by an alpine climate, with mean annual precipitation of 1220 mm, 49% of which falls as snow. Snowmelt plays a major role in controlling runoff in late spring but summer and early autumn rainfall events also represent an important contribution to the flow regime. Despite its small scale, the LCC spans a broad range of elevation (1970–2120 m a.s.l.), with the steepest slopes (up to 48°) in the upper portion (2050–2120 m a.s.l.) as well as in the lower portion (1970–2010 m a.s.l.) where the valley is very narrow. The central part of the catchment features a more gentle topography, especially in the 2030–2040 and 2010–2020 m a.s.l. ranges, where the soil is often saturated or close to saturation (as observed during several field surveys and also indicated by hydrophilic vegetation such as *Eriophorum scheuchzeri* and *Equisetum* sp.). The catchment is untouched by anthropic activities and is densely vegetated, with grassland, scattered shrubs, and a few trees (European larches and Norway spruces) mainly located on the ridges. The soil is classified as Cambisol with mull, with porosity ranging from 70.5% in the first 10 cm to 45.0% at 70 cm depth. Clay represents the highest contributor to the soil texture (up to 73% along the soil profile), followed by silt (up to 28%) and sand (up to 9%). For more detailed information on the study area, see *Penna et al*. [2009, 2010, 2011, 2013a, 2013b].

Hydrometeorological data were collected in the catchment from 11 April to 15 October 2007 and from 19 June to 31 October 2009. Rainfall was measured by a tipping bucket rain gauge (0.2 mm resolution) located


© 2014. American Geophysical Union. All Rights Reserved.

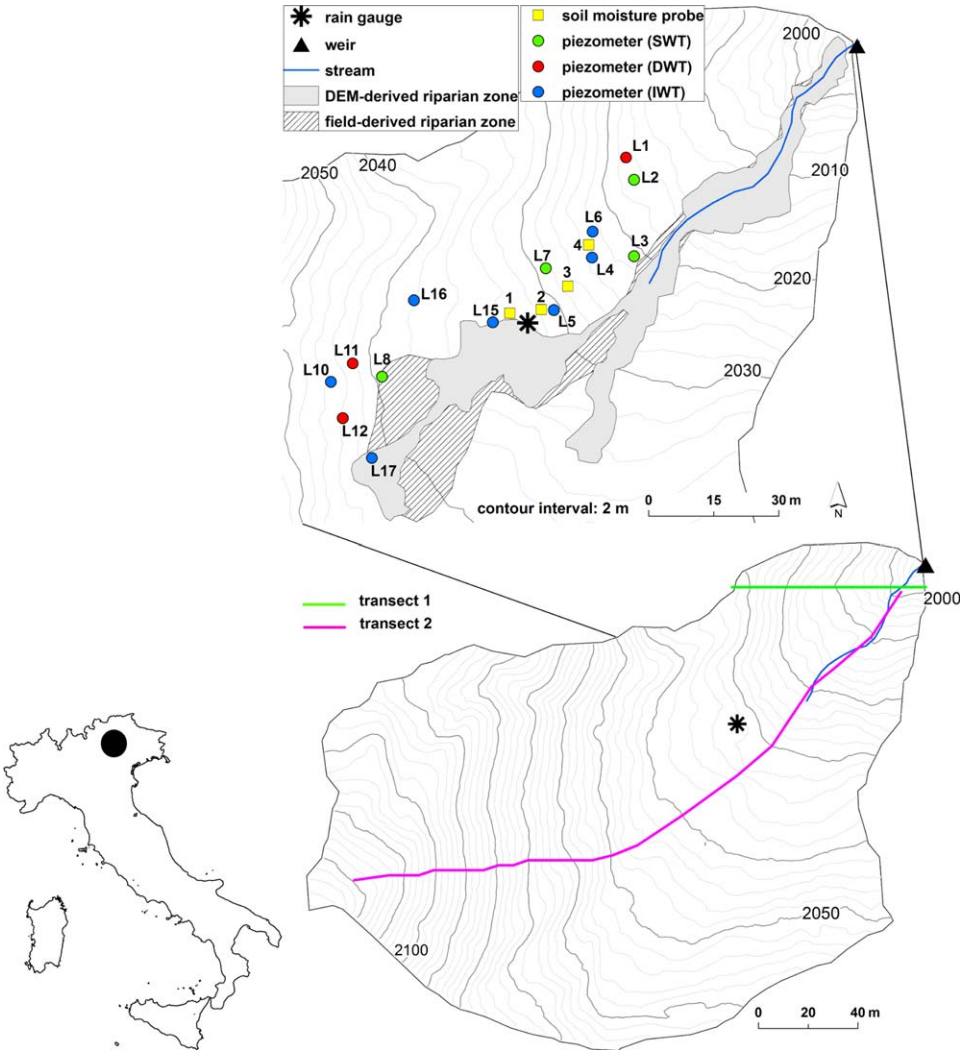


**Figure 1.** (bottom left) Map of the LCC showing its location within Italy, (bottom right) the two cross profiles (magenta and green lines) used for the virtual simulations, and (top) a zoom on the position of the instruments. The observation wells are grouped according to their average water table level (SWT: shallow water table; DWT: deep water table; IWT: intermediate water table).

at approximately 2030 m a.s.l. (Figure 1). Water stage in the stream was measured by a pressure transducer every 15 min at a 90° V-notch sharp-crested weir and then converted into discharge. Air temperature data were collected by a meteorological station located one km outside of the basin, at an altitude of 1940 m a.s.l., approximately 60 m below the position of the outlet. Water table variations were monitored by a network of observation wells (PVC pipes) equipped with capacitance rods, recording at a 15 min time step. Boreholes were drilled down to refusal and the depths of the observation wells ranged between 0.72 and 1.05 m. In 2007, 12 observation wells, labeled L1 to L12, were installed. Two of them (L2 and L9) were removed in 2009 due to instrument failure and three new ones (L15, L16, and L17) were added. Observation well L8 gave inconsistent results in 2007 and was excluded from the analysis and comparison with the model-simulated water table for that year. Volumetric water content averaged over the first 30 cm from the ground surface was measured at four locations in the central portion of the catchment by means of TDR (time domain reflectometry) probes recording at a 15 min time step. The records were then aggregated to 1 h intervals for data analysis. Soil moisture probes were removed at the end of the 2007 field campaign but were reinstalled in 2009 at exactly the same locations. A standard calibration suggested by the manufacturer for clay soils was applied. The position of all instruments is reported in Figure 1.

Two distinct topographic units can be identified in the catchment: (i) a riparian zone, characterized by high organic matter content and low hydraulic conductivity associated with the predominance of organic, silt,


© 2014. American Geophysical Union. All Rights Reserved.

and clay sized particles; and (ii) a hillslope zone, typically consisting of well-drained soils. The extent of the riparian areas within the catchment was estimated by integrating results from a DEM-threshold method and from field surveys. First, starting from a 1 × 1 m LiDAR resolution grid, flow accumulation (D∞ algorithm) was computed for the catchment, allowing for the identification of the cells belonging to the stream, above a threshold area of 3500 $m^2$. Then, riparian zones were identified as those flow accumulation cells characterized by a difference in elevation lower than 3 m compared to the stream cell they drained into [*Jencso et al*., 2009]. In the field, we traversed the whole catchment three times under different seasonal conditions (late spring, mid-summer, and early autumn), mapping all relatively flat areas that showed evidence of soil saturation or near-saturation, based on spatially distributed soil moisture measurements at 0–6 cm depth (Theta Probe, Delta-T Devices), vegetation characteristics, and visual observation. The topographic analysis and field survey methods yielded consistent results, especially in the lower part of the catchment where the stream lies. The extent of the riparian zone derived by the two methods is mapped in Figure 1.

Humid alpine catchments such as the LCC, characterized by shallow soils, rapid response to precipitation, and highly organized topographic structure and where fast subsurface flow is the dominant contributor to storm runoff, are ideal sites for studying the nonlinear dynamics of storage-discharge relationships [*McGlynn et al*., 2004; *Frisbee et al*., 2012].

### 2.2. The CATHY Model

The CATHY (CATchment HYdrology) model [*Camporese et al*., 2010] combines a three-dimensional equation for subsurface flow in variably saturated porous media (Richards equation) with a one-dimensional inertia-free approximation of the Saint Venant equations for surface water dynamics. The model belongs to a class of recently developed hydrological simulators that resolve in a numerically and dynamically consistent manner the interactions across the atmosphere-land surface-subsurface continuum (R. M. Maxwell et al., Surface–subsurface model intercomparison: A first set of benchmark results to diagnose integrated hydrology and feedbacks, submitted to *Water Resources Research*, 2013).

Spatial discretization in CATHY is built upon a DEM representing the catchment surface. The DEM cells are triangulated and replicated vertically to form a three-dimensional tetrahedral grid for the underlying soil and aquifer. Precipitation fluxes during storm events and potential evapotranspiration during interstorm periods are the main driving forces of the model. The model partitions this atmospheric forcing into surface runoff, infiltration, actual evapotranspiration, and changes in storage. Surface saturation or ponding can occur via the infiltration excess or saturation excess mechanisms, and both of these processes are automatically accounted for by a boundary condition switching algorithm that resolves the tight coupling between surface and subsurface flows. Overland flow is assumed to concentrate in rills or rivulets confined to "hillslope" cells, while channel flow occurs on "stream" cells. The distinction between overland and channel flow regimes is made using threshold-type relationships based on, for instance, upstream drainage area criteria [*Montgomery and Foufoula-Georgiou*, 1993]. The subsurface solver is based on Galerkin finite elements in space, a weighted finite difference scheme in time, and linearization via Picard iteration [*Paniconi and Putti*, 1994], whereas a nested explicit time discretization based on the Muskingum-Cunge scheme is used for the overland flow equation [*Orlandini and Rosso*, 1996].

Input for the model includes digital terrain data, surface-flow parameters such as Manning coefficients for hillslopes and channels, subsurface properties such as saturated hydraulic conductivity and soil retention curves, and atmospheric forcing terms (precipitation and potential evapotranspiration). The model-computed state variables include spatially distributed quantities (e.g., moisture content, surface and subsurface-flow velocities, aquifer water levels, and ponding heads) and integral quantities (e.g., streamflow at the catchment outlet and groundwater storage). A more detailed description of the CATHY model is given in *Camporese et al*. [2010].

## 3. Larch Creek Catchment: Modeled and Observed Storage-Discharge Dynamics

### 3.1. Model Setup

Starting from a 2 m × 2 m resolution DEM, the 3-D subsurface grid for the Larch Creek catchment was constructed by subdividing each DEM cell into two triangles and then projecting this 2-D surface mesh vertically for 1.05 m. A total of nine layers was used for the vertical discretization, with the layers progressively


© 2014. American Geophysical Union. All Rights Reserved.

coarser with depth to a maximum thickness of 0.16 m for the bottommost layer. The thinnest layer (0.04 m) at the surface is needed to accurately resolve rainfall-runoff-infiltration partitioning and in general to better capture the interactions between surface water and groundwater. The resulting 3-D grid contains 88,360 nodes and 464,130 tetrahedral elements.

The catchment was subdivided into riparian and hillslope zones representing the two main topographic units described in section 2.1 and shown in Figure 1. We simulated the two periods for which comprehensive field measurements are available, the first in 2007 (14 May to 15 October) for the calibration of the model parameters and the second in 2009 (7 July to 1 November) for validation. The atmospheric boundary conditions consisted of rainfall as measured by the rain gauge and evapotranspiration estimated by means of the Hargreaves-Samani formula [*Hargreaves and Samani*, 1982] on the basis of temperature data. No experimental evidence or geophysical information on possible bedrock fracturing or leakage is available at the site; and therefore, it is impossible to quantify the water flowing at the soil-bedrock interface. However, geological information for the area reveals that the substratum is made up mainly of massive limestone and compact dolomitic formations with little fracturing [*Van Beusekom*, 2004]. On this basis, we assumed no-flow conditions at the base of the soil domain. The lateral boundaries of the modeled domain were also assumed to be impermeable. The initial conditions were generated by running spin-up periods for the 2007 and 2009 simulations of 30 and 18 days, respectively, using measured rainfall rates and estimated evapotranspiration fluxes. Our numerical experiments showed that for the LCC spin-up periods of such duration are sufficient to obtain a state that is physically consistent and essentially unaffected by the conditions assigned at the beginning of the spin-up. The pressure head and surface discharge distributions at the end of the spin-up were then used as the initial conditions for the considered simulations.

### 3.2. Calibration and Validation of the Model Against Experimental Data

The instrumental setup in the LCC did not allow the water table dynamics in the riparian and hillslope zones to be discriminately monitored [*Seibert et al*., 2003] since only two observation wells (L8 and L17) were situated in the mapped riparian zone (Figure 1). Nonetheless quite different water table patterns within LCC were observed through the two monitoring years. Figure 2 presents a boxplot showing the distribution of water table data for 2007 and 2009 (for consistency in the comparison, only dates when all observation wells showed a water table value higher than the maximum monitoring depth were considered). Although groundwater depth within the catchment was characterized by a marked spatial variability, as also found in other experimental studies [e.g., *Haught and van Meerveld*, 2011; *Bachmair et al*., 2012; *Penna et al*., 2013b], some patterns did emerge. Three observation wells (L1, L11, and L12) gave consistently deep water table readings. Water table depth in four others was predominantly shallow or close to the soil surface (L2, L3, L7, and L8). The remaining observation wells showed an intermediate behavior. Interestingly, this pattern was preserved in both monitoring years, and the same grouping emerged from a cluster analysis (results not reported here). We designated these three piezometric categories as deep,

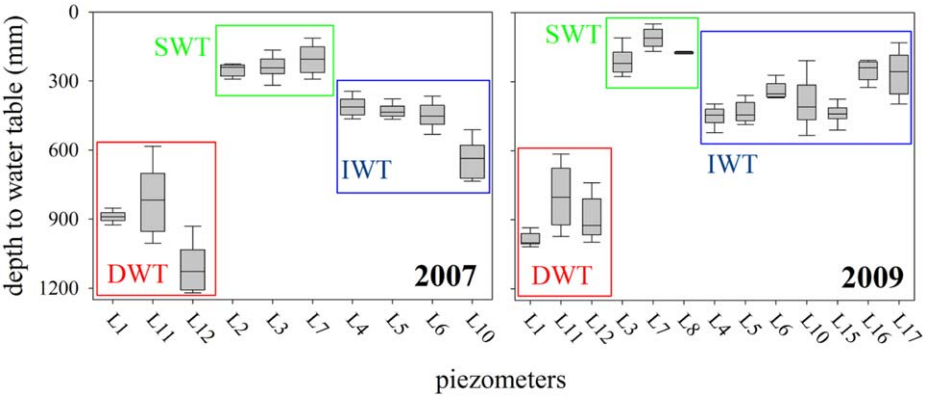


**Figure 2.** Boxplots of water table level in the observation wells for the (left) 2007 and (right) 2009 study periods. The boxes indicate the 25th and 75th percentiles, the whiskers indicate the 10th and 90th percentiles, and the horizontal line within the box marks the median. The red, green, and blue squares identify the observation wells with, respectively, deep, shallow, and intermediate average water table depth.


© 2014. American Geophysical Union. All Rights Reserved.

shallow, and intermediate water table zones (DWT, SWT, and IWT, respectively). The location of the observation wells partially explains the water level dynamics in the different groups, with the average distance between the observation wells and the stream decreasing from DWT to IWT to SWT.

As the focus of this study is to assess the capability of the model to reproduce the characteristics of storage-discharge relationships and not on achieving optimal predictive performance, a detailed multiparameter calibration was not needed and only a trial-and-error calibration of the hydraulic conductivity and specific storage was performed. This process yielded values of $K_s = 1.01 \times 10^{-2}$ m/h and $S_s = 5.18 \times 10^{-2}$ m$^{-1}$ for the riparian zone and $K_s = 1.46 \times 10^{-1}$ m/h and $S_s = 7.92 \times 10^{-3}$ m$^{-1}$ for the hillslope zone. The remaining parameters (porosity, retention curve constants, surface routing coefficients) were assigned on the basis of literature data and were assumed to be spatially homogeneous. Porosity is 0.55, residual water content is 0.108, and *van Genuchten* [1980] fitting parameters $\alpha$ and $n$ are 0.943 m$^{-1}$ and 1.35, respectively. The porosity value is intermediate between the minimum (0.45) and maximum (0.705) measured values. The set of subsurface parameters resulting from the calibration on the 2007 period is consistent with field observations carried out in very similar hillslopes located close to the LCC. *Penna et al.* [2013a] found that the average value of soil moisture along a 70 cm profile was 0.576 and that hillslope zone $K_s$ measured with a Guelph permeameter ranged between $2.9 \times 10^{-1}$ and $8.3 \times 10^{-2}$ m/h.

Figure 3 shows the comparison between simulated and measured data for the 14 May to 15 October 2007 and 7 July to 1 November 2009 periods. Water table depths are shown according to the observation well groupings described above, i.e., averaging the results for the observation wells with shallow, intermediate, and deep water tables. Soil moisture values are averaged over the four TDR locations and the top 30 cm of soil. A good match between simulated and measured data, for both the calibration and validation periods, is obtained for streamflow and soil moisture response, while the water table response is poorly matched in absolute terms but well captured in spatial dynamics. The simulated water levels preserve the shallow-

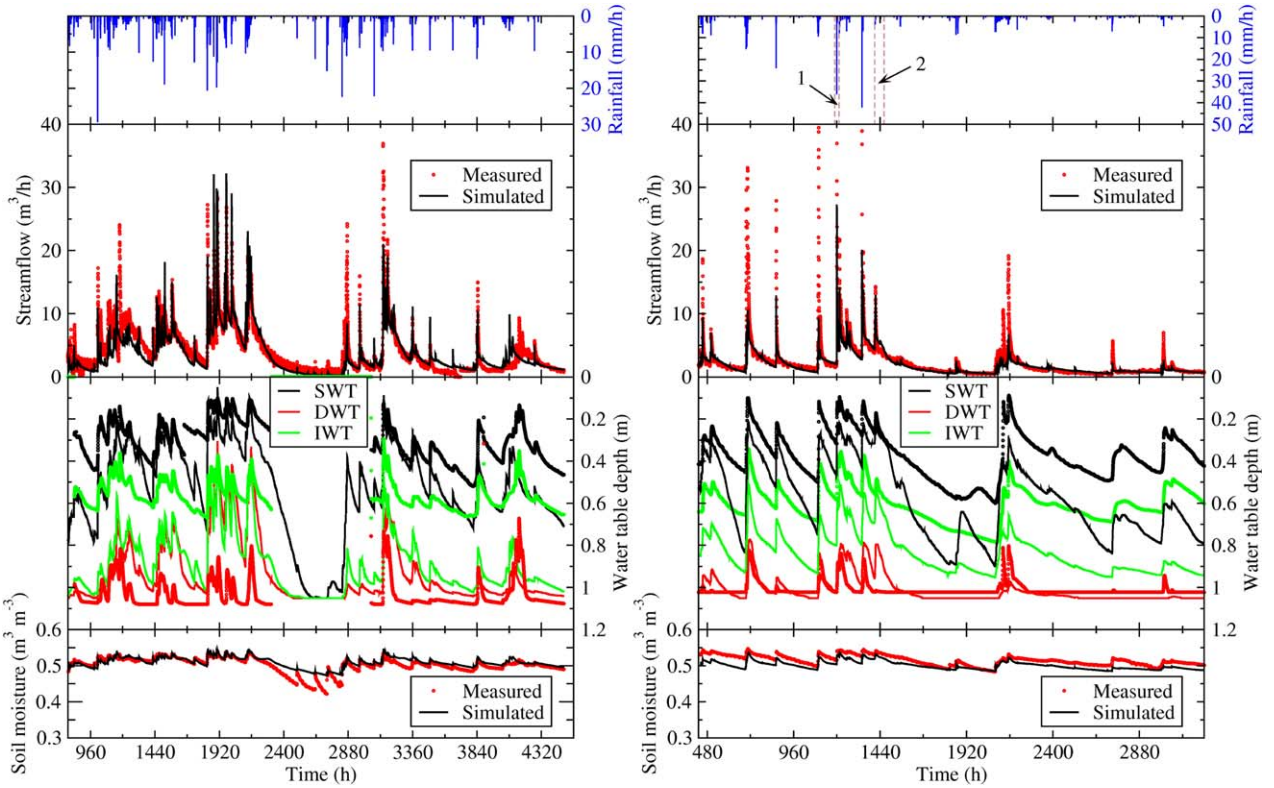


**Figure 3.** Comparison between simulated and measured data for (left) the 2007 simulation (14 May–15 October) and (right) the 2009 simulation (7 July–1 November). The time axes start at (left) 792 h and (right) 432 h (right) as the previous 33 and 18 days, respectively, are used for spin-up. Observations and simulations are denoted by unconnected circles and solid lines, respectively. The dashed vertical lines in the top right graph indicate the rainfall-runoff events considered for subsequent analyses of nonlinear behavior: (1) 7 and 8 August 2009 and (2) 16–18 August 2009.


© 2014. American Geophysical Union. All Rights Reserved.

intermediate-deep hierarchy, and the observed and simulated water table fluctuations are quite synchronous, except for a lag at the end of the 2007 simulation and a mismatch in deep response at around 1300–1400 h of the 2009 run. In the former case, the simulated water table peaks (as well as streamflow) anticipate the measured ones because of a snowfall event that the CATHY model treated as rainfall precipitation, whereas in the latter case a couple of DWT peaks simulated by the model are not recorded by the observation wells, perhaps due to deep infiltration into the bedrock that the model does not capture because of the no-flux boundary condition at the domain bottom. Note that, consistently with field observations [*Penna et al*., 2011, 2013b], the model generated surface runoff only through the mechanism of saturation from below, infiltration excess processes being negligible in this study area.

Table 1 summarizes the performance for the calibration and validation simulations evaluated by means of three different measures: the *Willmott* [1981] index of agreement (*WI*), the correlation coefficient *R*, and the root-mean-square error (*RMSE*). Parameter *WI* ranges from 0, indicating no agreement, to 1, which ensures a perfect reproduction, and is insensitive to a number of potential additive and proportional differences between observed and predicted values. For this reason, it is more suitable than the usual Nash-Sutcliffe coefficient to assess water table dynamics in our simulations. Note that the correlation coefficient consistently decreases from the shallow (0.79 and 0.87) to intermediate (0.73 and 0.76) to deep water table zones (0.45 and 0.58), suggesting that the model has some difficulty reproducing the water table dynamics close to the (hypothesized) bedrock.

### 3.3. Reproduction of Observed Storage-Discharge Dynamics

Figure 4 shows the simulated and measured hysteretic loops of the water table-streamflow relationships for the three groups of observation wells and for the rainfall-runoff events that occurred on 7 and 8 August 2009 and 16–18 August 2009. For consistency in the description of loop directions reported in the literature and in our own work, in this paper all storage-discharge relationships are interpreted in a reference frame with the storage variable plotted on the abscissa and the discharge variable on the ordinate. Although the measured and simulated data are not perfectly matched in absolute terms, the nonlinear dynamics is very well reproduced by the model for all three groups of observation wells. The only exception occurs for the DWT loop of the 16–18 August event, for which the measured loop is nearly invisible due to the lack of observation well response while the simulated loop is present and moreover consistent with the one of the 6–8 August event.

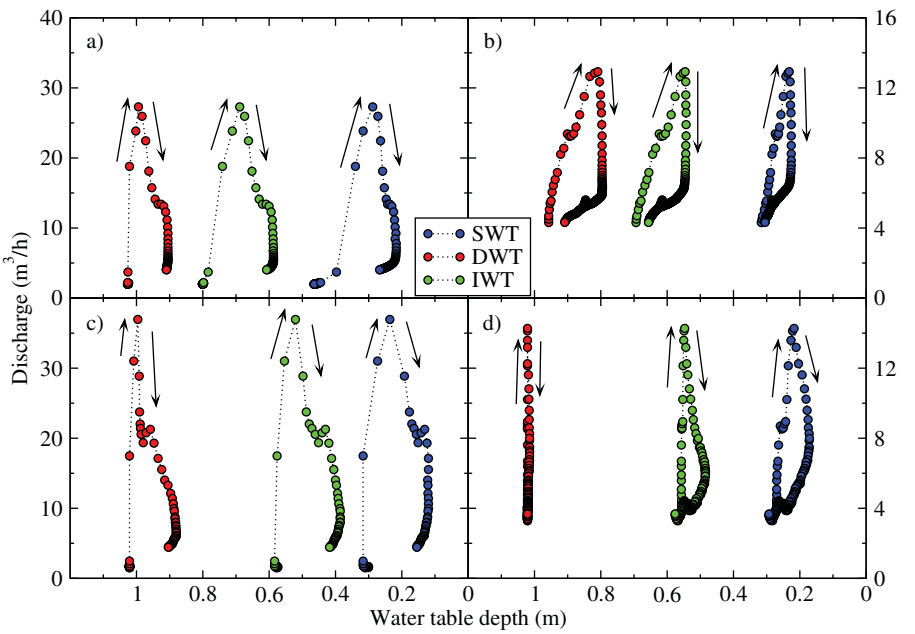


**Figure 4.** Nonlinear hysteretic relationship between discharge and water table depth for (a, b) simulated and (c, d) observed responses in the SWT, IWT, and DWT observation wells for the (a, c) 7 and 8 August 2009 and (b, d) 16–18 August 2009 rainfall events.


© 2014. American Geophysical Union. All Rights Reserved.

With the CATHY model, we can examine whether hysteresis also manifests itself in the subsurface storage-discharge relationship. Figure 5 shows the total subsurface storage, the saturated subsurface storage, and the unsaturated subsurface storage as a function of the streamflow discharge as simulated by the model during the rainfall-runoff events of 7 and 8 August 2009 and 16–18 August 2009. The hysteretic loops agree with the ones of the water table-discharge relationship and show that the dynamics is mainly controlled by the saturated zone. This can be seen in comparing the range of variation for total volume (∼20 mm for 7 and 8 August and ∼10 mm for 16–18 August) and for saturated storage (∼50 mm for 7 and 8 August and ∼30 mm for 16–18 August). Hysteresis in unsaturated storage versus discharge follows the dynamics of saturated storage but in the opposite direction (anti-clockwise loop) because as the water table rises (and thus saturated zone storage increases), the depth of the unsaturated zone (and thus its total storage) decreases.

An analogous hysteretic behavior can be observed when plotting the water table in the DWT-observation wells as a function of the same variable in the SWT cluster (Figure 6). Deep water tables are typically slower to respond than shallow water tables, but once triggered can rise rapidly, followed by a slow decrease during the recession phase. As a result, for the same SWT value, the DWT value is higher in the recession phase than in the rising limb of the hydrograph. Similar though less pronounced behavior is observed for IWT versus SWT water table depths. As can be seen in Figure 6, there is again good agreement between the observed data and the simulated dynamics.

## 4. Larch Creek Catchment: Synthetic Experiments

### 4.1. Model Setup

Several features of the experimental setup from the previous section impose constraints on the results obtained: instruments located mainly in the lower portion of the catchment, because sensors could not be easily installed on the steep slopes at higher elevations; a shallow soil of 1.05 m, conditioned by the depth to refusal of the observation wells; and an impermeable catchment base, thereby neglecting any bedrock leakage effects [e.g., *Broda et al*., 2011]. In this section, we present a series of virtual simulations that overcome these limitations. These additional experiments allow us to investigate the dependence of nonlinear processes on the properties of the catchment thickness and zonation (lateral heterogeneity). We also examine the response of the watershed along two transects, the first transversal to the stream flow direction and the second along the stream flow direction (transects 1 and 2, respectively, in Figure 1).

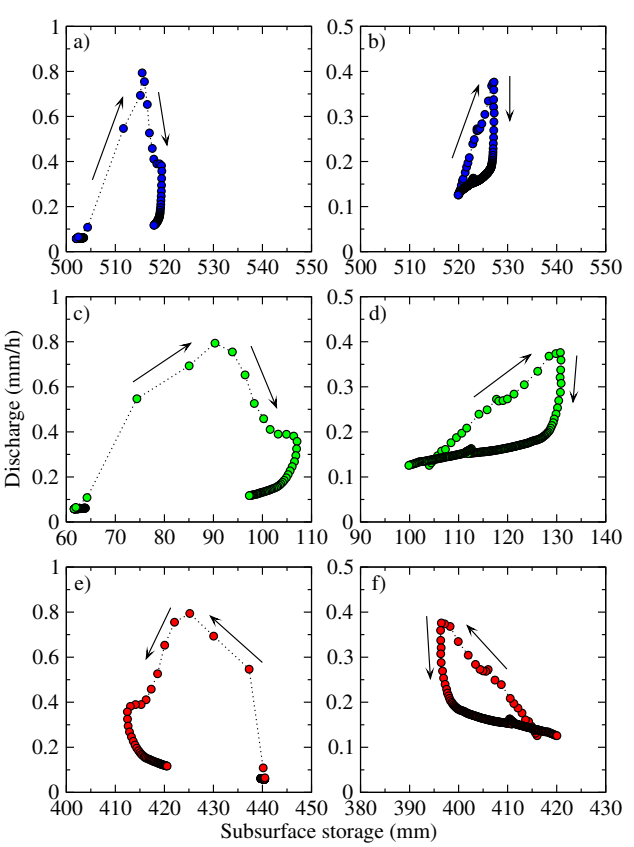


**Figure 5.** Nonlinear hysteretic relationship between (a, b) simulated discharge and total, (c, d) saturated, and (e, f) unsaturated subsurface storage for the (a, c, e) 7 and 8 August 2009 and (b, d, f) 16–18 August 2009 rainfall events.

We carried out eight simulation scenarios in which a thicker grid with a flat base is used for the study domain, simulating a soil deposit over a more or less impermeable bedrock. At the lowest topographic point, corresponding to the outlet of the catchment, a total thickness (surficial deposits plus bedrock aquifer) of 8.0 m was assigned to the three-dimensional finite element


© 2014. American Geophysical Union. All Rights Reserved.

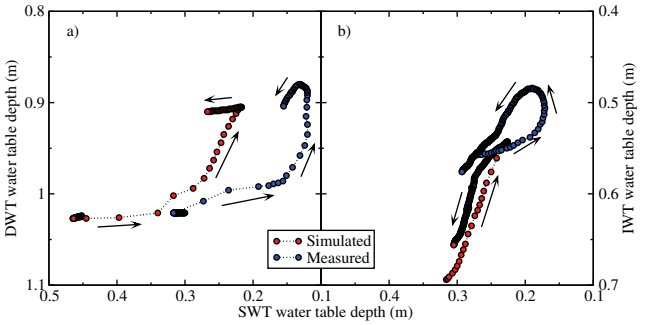


**Figure 6.** Nonlinear hysteretic relationships in simulated and observed water table responses between (a) SWT and DWT observation wells for the 7 and 8 August 2009 event and (b) SWT and IWT observation wells for the 16–18 August 2009 event.

grid. With a total topographic relief of 136 m for the catchment, the flat base configuration resulted in a maximum thickness (at the southern end of the catchment) of 144 m. A total of 15 layers was used for the vertical discretization, the top nine for the soil deposit and the last six for the underlying bedrock formation. Each layer, except the bottommost one, was aligned parallel to the surface and assigned a uniform thickness. The thinnest layer (0.04 m) is at the surface, as in the grid described in the previous section. The layers were progressively coarsened with depth, to a thickness of 1.29 m for layers 13 and 14. A thickness ranging from 3.07 m (north end of the catchment) to 138.86 m (south end) was assigned to the bottommost layer 15. As a consequence, the soil formation has a constant thickness of 1.05 m, while the underlying bedrock formation has a spatially variable thickness, from a minimum of 6.95 m at the northern tip of the watershed to a maximum of 142.95 m at the southern margin, where surface elevations are higher. In the first four scenarios (Table 2), the soil and bedrock are laterally homogeneous and the hydraulic conductivity of the six bedrock layers is progressively decreased from scenarios 1 to 4 so as to simulate increasing impermeability of the formation underlying the soil zone. From the fifth to the eighth scenarios (Table 2), the distinction between riparian and hillslope zones is maintained as in the previous section and the bedrock hydraulic conductivity is again progressively decreased.

Atmospheric forcing for the virtual simulations consisted of an initial 6 h period of $10^{-4}$ mm/h evaporation followed by a constant rainfall of 25 mm/h for 15 h and concluding with another period of evaporation at a rate of $10^{-4}$ mm/h until the end of the simulation. A long simulation period was used (5760 days) to fully capture the recession phase for all the scenarios. For the drainage episodes before and after the rain event, a very small evaporation rate was imposed instead of zero atmospheric forcing as this enhances numerical convergence in the CATHY model. Initial conditions for all scenarios were generated by a steady state simulation with the parameters of scenario 1, a high-constant rainfall rate of 0.228 mm/h (2000 mm/a), and a seepage face at the outlet to allow for groundwater outflow. Therefore, all the simulations started with the same pressure head distribution and wet conditions, ensuring that a large fraction of the catchment area contributes to runoff generation. As in the previous section, all runoff is generated by the saturation excess mechanism.

### 4.2. Simulation Results

Figure 7 shows the hysteretic loops between discharge and subsurface storage for the eight simulation scenarios described earlier (see also Table 2). The direction of the loops is always clockwise, but the shape changes according to the degree of imperviousness of the bedrock. As the hydraulic conductivity of the

**Table 1.** Performance Indices for the 2007 and 2009 Simulations of Streamflow, Water Table in the Three Different Zones, and Soil Moisture[a]

| | 2007 | | | 2009 | | |
|---|---|---|---|---|---|---|
| | WI | R | RMSE | WI | R | RMSE |
| Streamflow | 0.91 | 0.85 | 2.01 $m^3/h$ | 0.85 | 0.84 | 1.69 $m^3/h$ |
| SWT | 0.62 | 0.79 | 0.18 m | 0.60 | 0.87 | 0.23 m |
| DWT | 0.44 | 0.45 | 0.19 m | 0.69 | 0.58 | 0.05 m |
| IWT | 0.31 | 0.73 | 0.32 m | 0.42 | 0.76 | 0.24 m |
| Soil moisture | 0.85 | 0.87 | 0.01 | 0.73 | 0.89 | 0.02 |

[a]WI = *Willmott* [1981] index of agreement, R = correlation coefficient, RMSE = root-mean-square error. Time resolution of the data sets is 15 min for streamflow and water table, 1 h for soil moisture.


© 2014. American Geophysical Union. All Rights Reserved.

**Table 2.** Hydraulic Conductivity Values Used in the Numerical Experiments Carried Out With the Flat Bedrock Geometry

| | $K_{soil}$ (m/h) | | $K_{bedrock}$ (m/h) | |
|---|---|---|---|---|
| Scenario | Riparian | Hillslope | Riparian | Hillslope |
| 1 | $1.376 \times 10^{-1}$ | | $1.376 \times 10^{-1}$ | |
| 2 | $1.376 \times 10^{-1}$ | | $1.376 \times 10^{-2}$ | |
| 3 | $1.376 \times 10^{-1}$ | | $1.376 \times 10^{-3}$ | |
| 4 | $1.376 \times 10^{-1}$ | | $1.376 \times 10^{-4}$ | |
| 5 | $1.014 \times 10^{-2}$ | $1.464 \times 10^{-1}$ | $1.014 \times 10^{-2}$ | $1.464 \times 10^{-1}$ |
| 6 | $1.014 \times 10^{-2}$ | $1.464 \times 10^{-1}$ | $1.014 \times 10^{-2}$ | |
| 7 | $1.014 \times 10^{-2}$ | $1.464 \times 10^{-1}$ | $1.014 \times 10^{-3}$ | |
| 8 | $1.014 \times 10^{-2}$ | $1.464 \times 10^{-1}$ | $1.014 \times 10^{-4}$ | |

bedrock formation decreases, the bedrock aquifer becomes increasingly inaccessible for storage and the fraction of rainfall available for runoff increases, thus the range of variability of streamflow becomes progressively larger than the range of variability of storage. Note that the subsurface storage values are much higher than those shown in Figure 5, due to the much thicker domain and wetter conditions used in these simulations.

An analysis of the spatial variation of the water table response times was carried out for the two transects shown in Figure 1. Figure 8 shows the time at which the water table begins to respond to the rainfall event ("rise time") and the time at which the water table begins to drop ("fall time") as functions of the distance along the transects for scenarios 1–4, as well as the corresponding water table profiles at the rise and fall times. For the transverse transect ("1" in Figure 1), the 0 m coordinate corresponds to the watershed divide while the stream is located at approximately 60 m from the divide. For the longitudinal transect ("2" in Figure 1), 0 m corresponds to the watershed outlet, while 250 m is the watershed divide. The response of the streamflow hydrograph is perfectly synchronous with the rain event, beginning its rise at the start of rainfall (6 h) and its recession at the end of the event (21 h). For all four scenarios, the response times of the water table correspond to the streamflow response times for a portion of the transects close to the stream or outlet (from 20–30 to 80 m for transect 1 and from 0 to 40–50 m for transect 2), where the water table is very shallow or at the surface. At the edge of these regions, we discern a threshold point where there is a jump in response times corresponding to deeper water tables. Decreasing the bedrock hydraulic conductivity affects only the values of the water table rise and fall times, but not the threshold distance, which does not change for scenarios 2–4. Scenario 1 (fully homogeneous) is an exception, with the threshold distance occurring further upslope (transect 1) or upstream (transect 2), probably due to the larger hydraulic conductivity that allows a faster infiltration front and thus a faster response of the water table. The longitudinal profiles (transect 2) are consistent with field observations that found the water table to be practically at the surface up to a distance of about 50 m from the watershed outlet. These results are also consistent with analyses carried out in a Swedish till catchment by *Seibert et al.* [2003], who found that the correlation between groundwater levels and hillslope runoff was strong within the riparian zone (<35 m from the stream in their case) and dropped abruptly in the upslope zone (>60 m from the stream), resulting in different characteristic response times between upslope and stream/riparian groundwater.

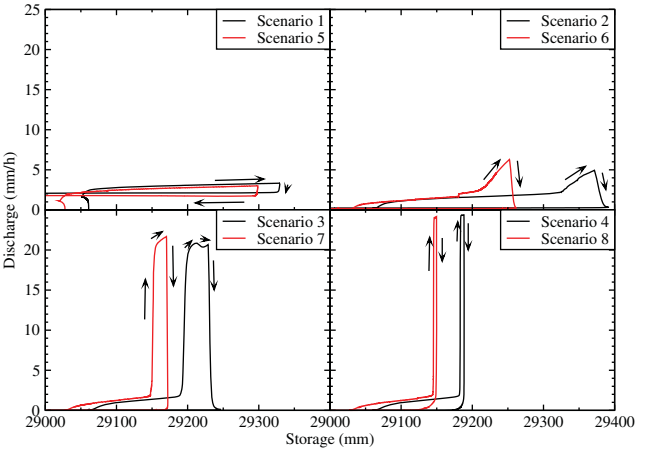


**Figure 7.** Hysteretic loops of the storage-discharge relationship for scenarios 1–8. The loops cover the entire simulation period (5760 days).

Figure 9 is analogous to Figure 8 but for scenarios 5–8, highlighting in this case the impact of lateral heterogeneity, since in these scenarios we attribute different


© 2014. American Geophysical Union. All Rights Reserved.

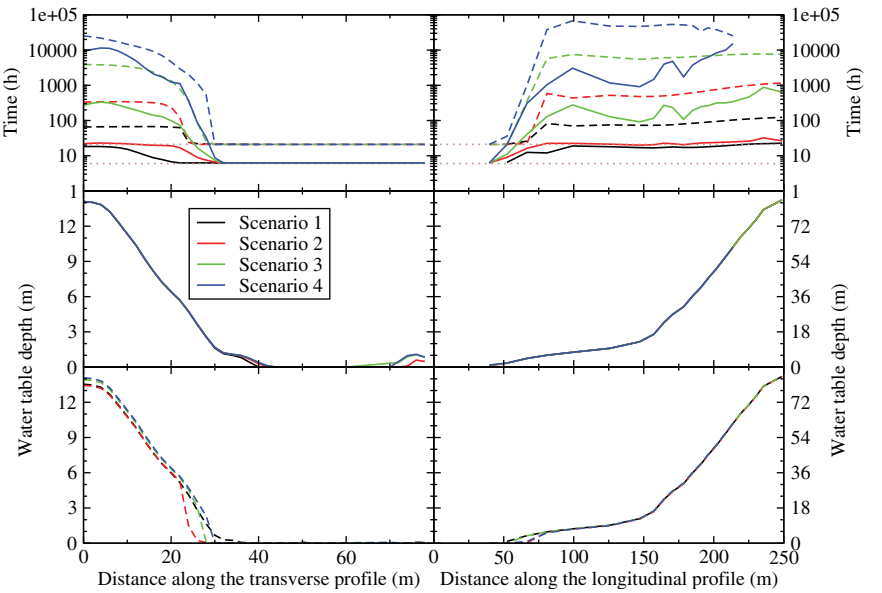


**Figure 8.** (top) Time at which the water table starts to rise (solid lines) and to fall (dashed lines) as a function of distance along the transverse and longitudinal transects (see Figure 1) for scenarios 1–4; (middle) Profile of water table depth at rise time; (bottom) Profile of water table depth at fall time. The dotted horizontal lines in the top graphs show the rise (6 h) and fall (21 h) times for the discharge response. Note that the water table depths in the middle and bottom plots refer to different times.

values to parameters $K_s$ and $S_s$ for the hillslope and riparian areas (Figure 1 and Table 2). The results are broadly consistent with those of scenarios 1–4 for the transverse profile (transect 1), as the riparian area coincides with the zone close to the stream regardless of the subsurface parameters. The major impact of the different soil properties is noticeable for the longitudinal profiles (transect 2), where the response times always exhibit a decrease in correspondence of the hillslope zone due to the higher hydraulic conductivity. This effect is more evident for scenarios 5 and 6, where the "sawtooth" trend is clearly visible, and tends to smooth out as the hydraulic conductivity of the bedrock decreases. The blue lines (Scenario 8) vanish at ~10 m in the transverse profiles and at ~200 m in the longitudinal profiles because beyond those points the water table does not show any response.

Figure 10 shows the simulated water table profiles along the transverse and longitudinal transects at the beginning and at the end of the simulations, along with the soil surface profiles. Comparing this figure with Figures 8 and 9, it appears that the main control on the response time is exerted by the local terrain slope. The threshold distances in Figures 8 and 9 coincide with points in Figure 10 where a significant change in slope first occurs (i.e., at a distance of ~30 m for the transverse profile and ~50 m for the longitudinal profile) and where the water table becomes increasingly deep. A second change in slope occurs at ~150 m for the longitudinal profile, with less dramatic but still apparent effects on the water table, especially in scenarios 3, 4, 7, and 8.

## 5. V-Shaped Catchment Synthetic Experiments

### 5.1. Model Setup

The v-catchment is formed by 81 × 81 DEM cells, 3 m × 3 m each, with three different topographic configurations: no riparian zone (DEM 1), a 9 m wide riparian zone (DEM 2), and a 21 m wide riparian zone (DEM 3). In DEM 1 (Figure 11), a single line of DEM cells at the valley bottom represents a straight creek or river, while in DEM 2 and DEM 3 the number of these cell lines is increased to three and seven, respectively. The catchment area is 59,049 $m^2$ and the slope is 30% along the $x$ coordinate and 3% along the $y$ coordinate. The soil depth increases linearly from 0.5 m at the divide to 1 m under the valley floor (as a consequence the average soil depth increases slightly from DEM 1 to DEM 2 to DEM 3). The three DEMs are intended to be simplified representations of the typical topography of small catchments in the study area.


© 2014. American Geophysical Union. All Rights Reserved.

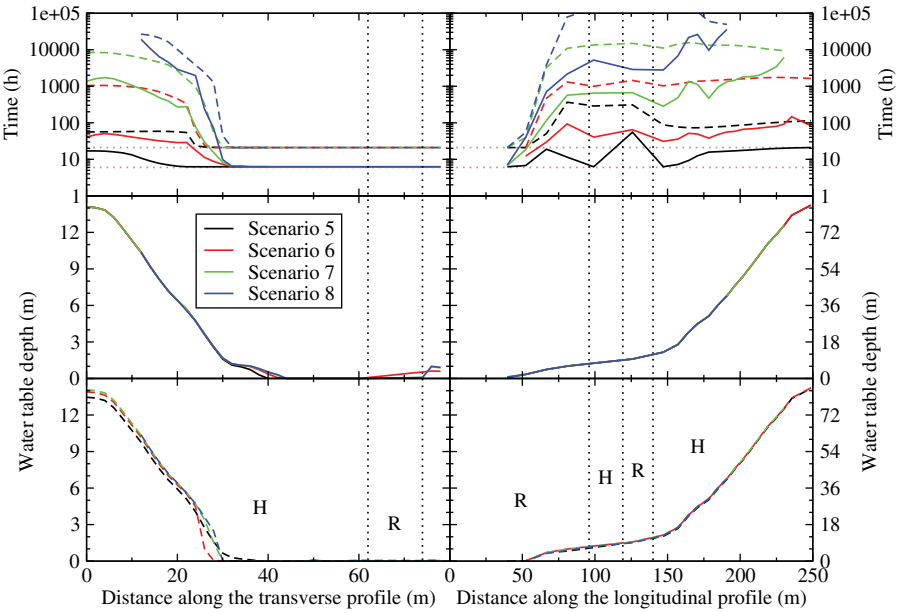


**Figure 9.** (top) Time at which the water table starts to rise (solid lines) and to fall (dashed lines) as a function of distance along the transverse and longitudinal transects (see Figure 1) for scenarios 5–8; (middle) Profile of water table depth at rise time; (bottom) Profile of water table depth at fall time. The dotted horizontal lines in the top graphs show the rise (6 h) and fall (21 h) times for the discharge response, while the dotted vertical lines demarcate riparian (R) and hillslope (H) zones, which have been assigned different hydraulic conductivities for these four scenarios. Note that the water table depths in the middle and bottom plots refer to different times.

The subsurface parameter values are equal to the ones described earlier in section 3.1, except for $K_s$ and $S_s$ which are now considered to be spatially homogeneous and equal to $1.46 \times 10^{-1}$ m/h and $7.92 \times 10^{-3}$ $m^{-1}$, respectively. The initial conditions consist of a 0.5 m deep water table under the creek/riparian zone and completely unsaturated hillsides. For each catchment, two storm scenarios are simulated with different rainfall durations but the same rainfall intensity (25 mm/h): Scenario 1, a long rainfall event (15 h) with the same atmospheric forcing described in section 4.1; and Scenario 2, a relatively short rainfall event (5 h, from $t = 6$ h to $t = 11$ h). In both scenarios, the simulation time is 1460 h (∼60 days).

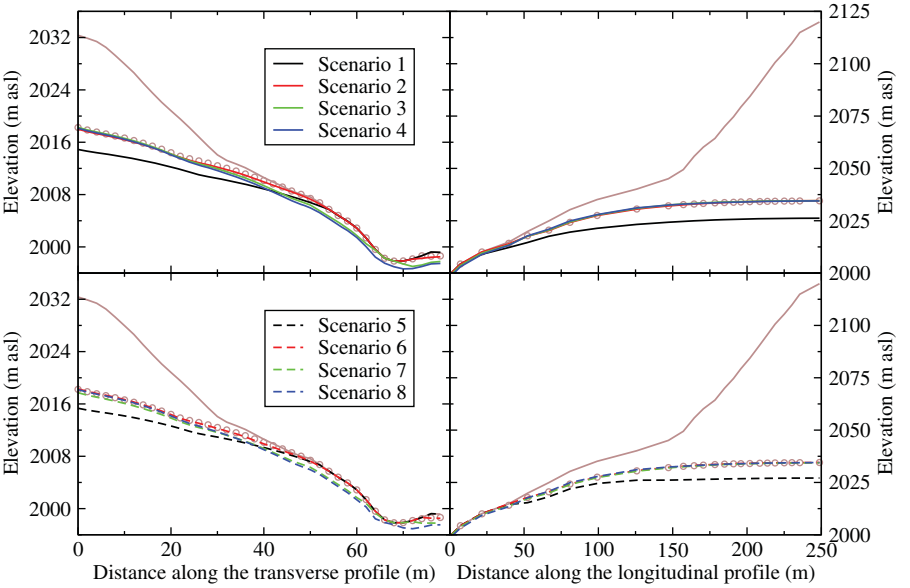


**Figure 10.** Soil profile elevation (solid brown lines), water table profile at the beginning of the simulations (circles), and water table profiles at the end of the simulations for scenarios 1–8.


© 2014. American Geophysical Union. All Rights Reserved.

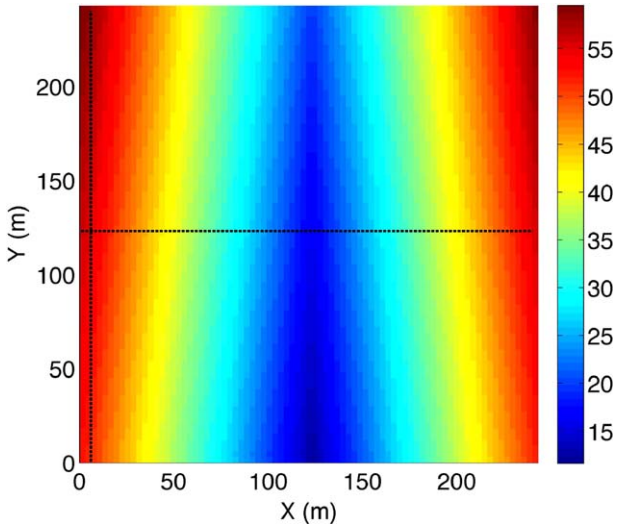


**Figure 11.** Digital elevation model (DEM) of the synthetic v-catchment with no riparian zone (DEM 1). Colorbar on the right denotes elevations in m. Dashed black lines indicate two transects used for the subsequent analysis of water table response times. DEM 2 and DEM 3 (not shown) have similar topography but with a 9 and 21 m wide riparian zone, respectively.

### 5.2. Simulation Results

Figures 12a and 12c show the dimensionless streamflow hydrograph for the three v-catchments and two scenarios. Streamflow normalization is achieved by dividing the computed discharge by the maximum possible discharge, i.e., 59,049 $m^2 \times 0.025$ m/h = 1476.2 $m^3$/h, which can be reached only when the catchment is completely saturated. In Scenario 1, the three catchments saturated completely due to the long rainfall duration, and surface runoff generated by saturation from below was triggered in the riparian zone as well as in the hillslopes. In Scenario 2, the three catchments partially saturated and only a small portion around the riparian zone experienced a water table response. The main differences between the three configurations are manifest particularly in Scenario 2, where DEM 3 shows a higher rate of discharge increase in the rising limb of the hydrograph compared to DEM 2 and DEM 1. This is due to the wider riparian zone, which reacts quickly to the rainfall event and leads to a higher peak discharge. The same process can also be observed in Scenario 1, where, starting from about $t = 11$ h, the hillslopes begin to saturate and the rising limbs in the three hydrographs display a significant deceleration leading eventually to a merging of the three curves.

Figures 12b and 12d show the dimensionless storage-discharge relationships for the three v-catchments and two scenarios. Storage normalization is achieved by dividing the computed total storage by the maximum water that could be stored in the basin at saturation. As for the Larch Creek simulations, the hysteretic loops are always in a clockwise direction. The differences in hysteretic behavior between the three v-catchments are more significant in Scenario 2 than in Scenario 1. This is because for the relatively short rain event of Scenario 2 surface runoff was generated almost exclusively in the riparian area, whereas for the long event of Scenario 1 the hillslope zone also generated runoff and the relative importance of the riparian zone decreased.

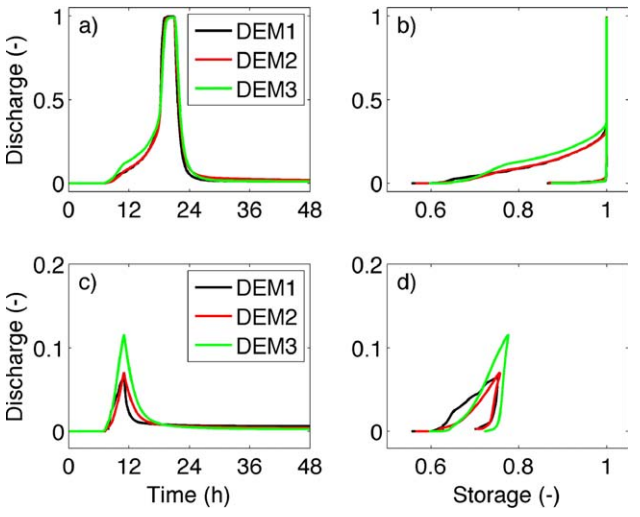


**Figure 12.** (a and c) Streamflow hydrographs and (b and d) storage-discharge relationships for (a and b) Scenario 1 (long rainfall event) and (c and d) Scenario 2 (short rainfall event) for the three v-catchments. Discharge and storage are normalized as described in section 5.2.. The curves in Figures 12b and 12d are in the clockwise direction.

The same analysis of the spatial variation of water table response time described in section 4.2 was repeated for Scenario 1, for which the rainfall event is long enough to trigger a response over the whole catchment.


© 2014. American Geophysical Union. All Rights Reserved.

Figure 13 shows the time at which the water table begins to rise in response to the rainfall event in the transverse transect (Figure 13a) and in the longitudinal transect (Figure 13b) (the transects can be seen in Figure 11). Figure 13a clearly demonstrates the impact of the riparian zone width on the water table dynamics, with a very quick response within the riparian zone and a significant increase in rise time as soon as the terrain starts to climb. The numerical artifact on the left edges of the curves is due to proximity to the boundary. Figure 13b, which shows the water table response along the longitudinal transect, highlights the impact of soil depth on the water table dynamics. The water table response in the hillslopes slows down slightly as the width of the riparian zone increases, in correspondence to the soil growing gradually thicker from DEM 1 to DEM 2 to DEM 3.

In summary, the simulation results with the simplified geometry of the synthetic v-catchments confirm what was found previously for the more complex LCC, i.e., that topography is the primary factor controlling the nonlinear characteristics of the storage-discharge relationship. This control is exerted primarily through the distinction between a riparian zone, normally characterized by shallow water table and fast response, and a hillslope zone, whose response, once triggered by large enough rainfall events, contributes significantly to runoff generation.

## 6. Summary and Conclusions

A three-dimensional Richards equation-based hydrological model, CATHY, applied to a mountain headwater catchment in the Italian Alps has been shown to be able to reproduce complex nonlinear behaviors, such as thresholding and hysteretic storage-discharge relationships, observed in the field. No ad hoc parameterization of soil hysteresis or other possible controlling mechanism was introduced into the model. Process-based distributed models of surface/subsurface water flow such as CATHY are thus useful tools for probing the mechanisms of streamflow generation at the hillslope and catchment scales.

In the LCC, hysteresis is the result of different response times between hydrological processes that involve fast surface flows and slower subsurface flows. This difference in response times creates hysteretic behavior in the relation between streamflow and storage that is shown to be typically characterized by a clockwise direction of the loops (i.e., streamflow response is faster than storage response). So for instance, for the same discharge value and taking water table level as the storage variable, the water table will be higher in the recession phase than during the rising limb of the hydrograph, due to the slower response of groundwater to a rainfall event. In other results, the CATHY simulations suggest that soil moisture is more persistent than streamflow, especially in catchment locations where the water table tends to be shallow (e.g., in riparian areas), since in these near-stream regions upslope water is still being redistributed after a rainfall event. These downslope zones typically have a large drainage or contributing area and stay wet even after rainfall and during streamflow recession due to subsurface soil moisture redistribution.

Such behavior was also found in other experimental catchments with similar physiographic properties [e.g., *Myrabø*, 1997; *Kendall et al*., 1999; *McGlynn et al*., 2004; *Lana-Renault et al*., 2013], where the organization and the distribution of dominant landscape features were identified as the main controlling factors for the storage-discharge relationship. A common theme that emerges in these studies is the importance of the hydrological connectivity between the different landscape features (i.e., hillslope and riparian zone), which is often ascribed to macropore flow or other preferential pathways. We show here that empirically observed connectivity dynamics can be simulated without resorting to such mechanisms.

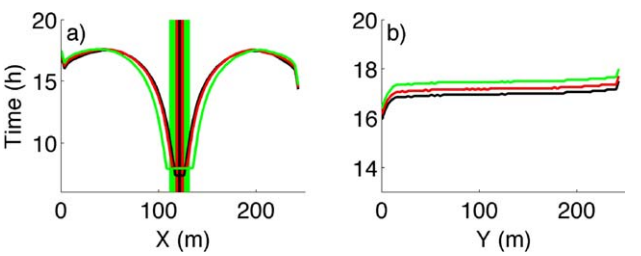


**Figure 13.** Water table response time (time at which the water table begins to rise) for DEM 1 (black), DEM 2 (red), and DEM 3 (green) along (a) the transect transversal to the creek/riparian zone and (b) the longitudinal transect. The black, red, and green bands in the middle of Figure 13a represent width and position of the creek/riparian areas for DEM 1, DEM 2, and DEM 3, respectively. Ground surface elevation in Figure 13b increases from X = 0 m (downstream) to X = 240 m (upstream).

Additional numerical experiments were also carried out for a synthetic rainfall-runoff event to investigate the effects of aquifer


© 2014. American Geophysical Union. All Rights Reserved.

thickness, bedrock leakage, and soil heterogeneity (in particular the distinction between riparian and hillslope zones) on catchment response and nonlinear behavior. The results confirm that the primary control on the nonlinear catchment response is exerted by topography. Soil heterogeneity (represented here as lateral zonation) and bedrock imperviousness play a secondary role, affecting only the values of the variables of interest (water table levels and streamflow discharge) and the response times, but not the general nonlinear patterns.

The findings from the Larch Creek simulations are corroborated by a final series of numerical experiments carried out for a simple v-shaped catchment in three topography configurations: no riparian zone, a 9 m wide riparian zone, and a 21 m wide riparian zone. During very wet conditions (caused by a long rainfall event), when the catchments are saturated, hillslope-riparian flowpaths are activated, water is transmitted rapidly from the hillslopes through the riparian zone to the stream, the time lag between streamflow and storage is reduced, and differences in the hysteretic behavior between the three topographies are less manifested. Conversely, during dry or relatively dry conditions (smaller/shorter rainfall events), only riparian groundwater or groundwater at the bottom of the hillslope responds, the hillslope contribution to runoff is limited, water flows are slower, the time lag between streamflow and storage increases, and differences in the hysteretic behavior between the three configurations are more marked. The results of the v-catchment experiments, which are not affected by factors such as soil or bedrock aquifer heterogeneity, confirm that topography and soil depth exert a strong control on nonlinear storage-discharge dynamics. Our modeling results at the LCC are consistent with field observations, hydrometric measurements, and tracer tests conducted in the same study area [*Penna et al*., 2011, 2013a, 2013b] and provide a new perspective on the internal functioning of humid catchments.

**Acknowledgments**

This work was financially supported by the research project GEO-RISKS (University of Padua, STPD08RWBY) and the project "Giovani Studiosi—Ricerche di carattere innovative e di eccellenza proposte da giovani non strutturati, decreto rettorale n. 800–2011, 23/03/2011, Università degli Studi di Padova, Dipartimento Territorio e Sistemi Agroforestali." We thank Alberto De Luca (Geomatica e Ambiente, University of Padua) for developing the GIS-based algorithm for the computation of the riparian zone extent. We also wish to thank the three anonymous reviewers for their detailed and very helpful comments.

## References

Allen, D. M., P. H. Whitfield, and A. Werner (2010), Groundwater level responses in temperate mountainous terrain: Regime classification, and linkages to climate and streamflow, *Hydrol. Processes*, *24*, 3392–3412, doi:10.1002/hyp.7757.

Bachmair, S., M. Weiler, and P. A. Troch (2012), Intercomparing hillslope hydrological dynamics: Spatio-temporal variability and vegetation cover effects, *Water Resour. Res.*, *48*, W05537, doi:10.1029/2011WR011196.

Beven, K. (2006), Searching for the Holy Grail of scientific hydrology: Qt = H(S, R, Δt)A as closure, *Hydrol. Earth Syst. Sci.*, *10*, 609–618.

Bixio, A. C., G. Gambolati, C. Paniconi, M. Putti, V. M. Shestopalov, V. N. Bublias, A. S. Bohuslavsky, N. B. Kastelteseva, and Y. F. Rudenko (2002), Modeling groundwater-surface water interactions including effects of morphogenetic depressions in the Chernobyl exclusion zone, *Environ. Geol.*, *42*, 162–177.

Broda, S., C. Paniconi, and M. Larocque (2011), Numerical investigation of leakage in sloping aquifers, *J. Hydrol.*, *409*, 49–61, doi:10.1016/j.jhydrol.2011.07.035.

Camporese, M., C. Paniconi, M. Putti, and S. Orlandini (2010), Surface-subsurface flow modeling with path-based runoff routing, boundary condition-based coupling, and assimilation of multisource observation data, *Water Resour. Res.*, *46*, W02512, doi:10.1029/2008WR007536.

Detty, J. M., and K. J. McGuire (2010a), Topographic controls on shallow groundwater dynamics: Implications of hydrologic connectivity between hillslopes and riparian zones in a till mantled catchment, *Hydrol. Processes*, *24*, 2222–2236.

Detty, J. M., and K. J. McGuire (2010b), Threshold changes in storm runoff generation at a till-mantled headwater catchment, *Water Resour. Res.*, *46*, W07525, doi:10.1029/2009WR008102.

Dooge, J. C. I. (2005), Bringing it all together, *Hydrol. Earth Syst. Sci.*, *9*(1–2), 3–14.

Ewen, J., and S. J. Birkinshaw (2007), Lumped hysteretic model for subsurface stormflow developed using downward approach, *Hydrol. Processes*, *21*, 1496–1505, doi:10.1002/hyp.6344.

Frei, S., G. Lischeid, and J. H. Fleckenstein (2010), Effects of micro-topography on surface–subsurface exchange and runoff generation in a virtual riparian wetland: A modeling study, *Adv. Water Resour.*, *33*, 1388–1401.

Frisbee, M. D., F. M. Phillips, G. D. Weissmann, P. D. Brooks, J. L. Wilso, A. R. Campbell, and F. Liu (2012), Unraveling the mysteries of the large watershed black box: Implications for the streamflow response to climate and landscape perturbations, *Geophys. Res. Lett.*, *39*, L01404, doi:10.1029/2011GL050416.

Gauthier, M.-J., M. Camporese, C. Rivard, C. Paniconi, and M. Larocque (2009), A modeling study of heterogeneity and surface water–groundwater interactions in the Thomas Brook catchment, Annapolis Valley (Nova Scotia, Canada), *Hydrol. Earth Syst. Sci.*, *13*, 1583–1596, doi:10.5194/hess-13-1583-2009.

Guay, C., M. Nastev, C. Paniconi, and M. Sulis (2013), Comparison of two modeling approaches for groundwater–surface water interactions, *Hydrol. Processes*, *27*(16), 2258–2270, doi:10.1002/hyp.9323.

Hargreaves, G. H., and Z. A. Samani (1982), Estimating potential evapotranspiration, *J. Irrig. Drain. Eng.*, *108*(3), 225–230.

Haught, D. R. W., and H. J. van Meerveld (2011), Spatial variation in transient water table responses: Differences between an upper and lower hillslope zone, *Hydrol. Processes*, *25*, 3866–3877.

Hill, A. R. (1996), Nitrate removal in stream riparian zones, *J. Environ. Qual.*, *25*, 743–755.

Jencso, K. J., B. L. McGlynn, M. N. Gooseff, S. M. Wondzell, K. E. Bencala, and A. Marshall (2009), Hydrologic connectivity between landscapes and streams: Transferring reach- and plot-scale understanding to the catchment scale, *Water Resour. Res.*, *45*, W04428, doi:10.1029/2008WR007225.

Kendall, K. A., J. B. Shanley, and J. J. McDonnell (1999), A hydrometric and geochemical approach to test the transmissivity feedback hypothesis during snowmelt, *J. Hydrol.*, *219*, 188–205.


© 2014. American Geophysical Union. All Rights Reserved.

Lana-Renault, N., D. Regüés, P. Serrano, and J. Latron (2013), Spatial and temporal variability of groundwater dynamics in a sub-Mediterranean mountain catchment, *Hydrol. Processes*, doi:10.1002/hyp.9892.
Latron, J., and F. Gallart (2008), Runoff generation processes in a small Mediterranean research catchment (Vallcebre, Eastern Pyrenees), *J. Hydrol.*, *358*, 206–220.
Lehmann, P., C. Hinz, G. McGrath, H. J. Tromp-van Meerveld, and J. J. McDonnell (2007), Rainfall threshold for hillslope outflow: An emergent property of flow pathway connectivity, *Hydrol. Earth Syst. Sci.*, *11*, 1–17.
McGlynn, B. L., J. J. McDonnell, J. Seibert, and C. Kendall (2004), Scale effects on headwater catchment runoff timing, flow sources, and groundwater-streamflow relations, *Water Resour. Res.*, *40*, W07504, doi:10.1029/2003WR002494.
McGuire, K. J., and J. J. McDonnell (2010), Hydrological connectivity of hillslopes and streams: Characteristic timescales and nonlinearities, *Water Resour. Res.*, *46*, W10543, doi:10.1029/2010WR009341.
Mishra, S. K., and V. P. Singh (1999), Hysteresis-based flood wave analysis, *J. Hydrol. Eng.*, *4*(4), 358–365.
Montgomery, D. R., and E. Foufoula-Georgiou (1993), Channel network source representation using digital elevation models, *Water Resour. Res.*, *29*(12), 3925–3934.
Myrabø, S. (1997), Temporal and spatial scale of response area and groundwater variation in a till, *Hydrol. Processes*, *11*, 1861–1880.
Norbiato, D., and M. Borga (2008), Analysis of hysteretic behaviour of a hillslope-storage kinematic wave model for subsurface flow, *Adv. Water Resour.*, *31*, 118–131.
O'Kane, J. P., and D. Flynn (2007), Thresholds, switches and hysteresis in hydrology from the pedon to the catchment scale: A non-linear systems theory, *Hydrol. Earth Syst. Sci.*, *11*(1), 443–459.
Orlandini, S., and R. Rosso (1996), Diffusion wave modeling of distributed catchment dynamics, *J. Hydraul. Eng.*, *1*(3), 103–113.
Paniconi, C., and M. Putti (1994), A comparison of Picard and Newton iteration in the numerical solution of multidimensional variably saturated flow problems, *Water Resour. Res.*, *30*(12), 3357–3374.
Penna, D., M. Borga, D. Norbiato, and G. Dalla Fontana (2009), Hillslope scale soil moisture variability in a steep alpine terrain, *J. Hydrol.*, *364*, 311–327, doi:10.1016/j.jhydrol.2008.11.009.
Penna, D., M. Borga, M. Sangati, and A. Gobbi (2010), Dynamics of soil moisture, subsurface flow and runoff in a small alpine basin, in *Proceedings of the Workshop Held at Goslar-Hahnenklee on Status and Perspectives of Hydrology in Small Basins, IAHS Red Book Ser. 336*, pp. 96–102, IAHS, Wallingford, U. K.
Penna, D., H. J. Tromp-van Meerveld, A. Gobbi, M. Borga, and G. Dalla Fontana (2011), The influence of soil moisture on threshold runoff generation processes in an alpine headwater catchment, *Hydrol. Earth Syst. Sci.*, *15*, 689–702, doi:10.5194/hess-15-689-2011.
Penna, D., L. Brocca, M. Borga, and G. Dalla Fontana (2013a), Soil moisture temporal stability at different depths on two alpine hillslopes during wet and dry periods, *J. Hydrol.*, *477*, 55–71, doi:10.1016/j.jhydrol.2012.10.052.
Penna, D., N. Mantese, L. Hopp, G. Dalla Fontana, and M. Borga (2013b), Spatio-temporal variability of piezometric response on two alpine hillslopes, *Hydrol. Processes*, doi: 10.1002/hyp.10140.
Phillips, J. D. (2003), Sources of nonlinearity and complexity in geomorphic systems, *Prog. Phys. Geogr.*, *27*(1), 1–23, doi:10.1191/0309133303pp340ra.
Radatz, T. F., A. M. Thompson, and F. W. Madison (2013), Soil moisture and rainfall intensity thresholds for runoff generation in southwestern Wisconsin agricultural watersheds, *Hydrol. Processes*, *27*, 3521–3534, doi:10.1002/hyp.9460.
Seibert, J., K. Bishop, A. Rodhe, and J. J. McDonnell (2003), Groundwater dynamics along a hillslope: A test of the steady state hypothesis, *Water Resour. Res.*, *39*, 1014, doi:10.1029/2002WR001404.
Seibert, J., T. Grabs, S. Koeler, H. Laudon, M. Winterdahl, and K. Bishop (2009), Linking soil- and stream-water chemistry based on a Riparian Flow-Concentration Integration Model, *Hydrol. Earth Syst. Sci.*, *13*, 2287–2297.
Sidle, R. C., Y. Tsuboyama, S. Noguchi, I. Hosoda, M. Fujieda, and T. Shimizu (2000), Stormflow generation in steep forested headwaters: A linked hydrogeomorphic paradigm, *Hydrol. Processes*, *14*, 369–385.
Sulis, M., C. Paniconi, and M. Camporese (2011a), Impact of grid resolution on the integrated and distributed response of a coupled surface–subsurface hydrological model for the des Anglais catchment, Quebec, *Hydrol. Processes*, *25*(12), 1853–1865, doi:10.1002/hyp.7941.
Sulis, M., C. Paniconi, C. Rivard, R. Harvey, and D. Chaumont (2011b), Assessment of climate change impacts at the catchment scale with a detailed hydrological model of surface-subsurface interactions and comparison with a land surface model, *Water Resour. Res.*, *47*, W01513, doi:10.1029/2010WR009167.
Tromp-van Meerveld, H. J., and J. J. McDonnell (2006a), Threshold relations in subsurface stormflow: 1: A 147-storm analysis of the Panola hillslope, *Water Resour. Res.*, *42*, W02410, doi:10.1029/2004WR003778.
Tromp-van Meerveld, H. J., and J. J. McDonnell (2006b), Threshold relations in subsurface stormflow: 2: The fill and spill hypothesis, *Water Resour. Res.*, *42*, W02411, doi:10.1029/2004WR003800.
Van Beusekom, M. (2004), *A Hydrogeological Inventory of the Bacino del Cordevole, Northern Italy*, Fac. of Earth and Life Sci., Free Univ. of Amsterdam, Amsterdam.
van Genuchten, M. Th. (1980), A closed-form equation for predicting the hydraulic conductivity of unsaturated soils, *Soil Sci. Soc. Am. J.*, *44*, 892–898.
Vidon, P. (2011), Towards a better understanding of riparian zone water table response to precipitation: Surface water infiltration, hillslope contribution or pressure wave processes? *Hydrol. Processes*, *26*(21), 3207–3215, doi:10.1002/hyp.8258.
Weill, S., M. Altissimo, G. Cassiani, R. Deiana, M. Marani, and M. Putti (2013). Saturated area dynamics and streamflow generation from coupled surface–subsurface simulations and field observations, *Adv. Water Resour.*, *59*, 196–208, doi:10.1016/j.advwatres.2013.06.007.
Wenninger, J., S. Uhlenbrook, N. Tilch, and C. Leibundgut (2004), Experimental evidence of fast groundwater responses in a hillslope/floodplain area in the Black Forest Mountains, Germany, *Hydrol. Processes*, *18*, 3305–3322.
Willmott, C. J. (1981), On the validation of models, *Phys. Geogr.*, *2*, 184–194.
Zehe, E., T. Graeff, M. Morgner, A. Bauer, and A. Bronstert (2010), Plot and field scale soil moisture dynamics and subsurface wetness control on runoff generation in a headwater in the Ore Mountains, *Hydrol. Earth Syst. Sci.*, *14*, 873–889, doi:10.5194/hess-14-873-2010.


© 2014. American Geophysical Union. All Rights Reserved.